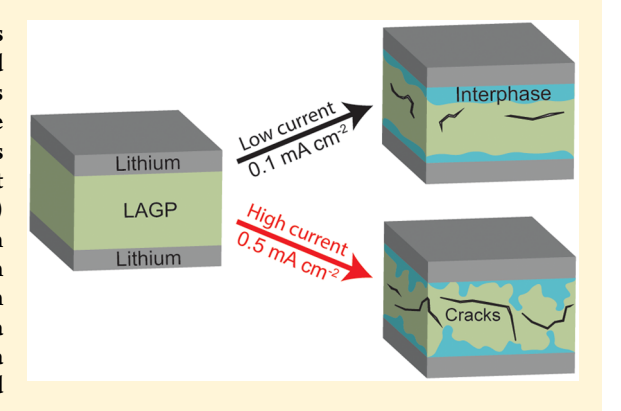


# Interphase Morphology between a Solid-State Electrolyte and Lithium Controls Cell Failure

John A. Lewis,<sup>†</sup> Francisco Javier Quintero Cortes,<sup>†</sup> Matthew G. Boebinger,<sup>†</sup> Jared Tippens,<sup>‡</sup> Thomas S. Marchese,<sup>†</sup> Neha Kondekar,<sup>†</sup> Xiaoming Liu,<sup>§</sup> Miaofang Chi,<sup>§</sup> and Matthew T. McDowell\*,<sup>†</sup>,<sup>‡</sup>

Supporting Information

ABSTRACT: The interfaces between many solid-state electrolytes (SSEs) and lithium metal are (electro)chemically unstable, and improved understanding of how interfacial transformations influence electrochemical degradation is necessary to stabilize these interfaces and therefore enable a wider range of viable SSEs for batteries. Here, the (electro)chemical reaction processes that occur at the interface between Li<sub>1.4</sub>Al<sub>0.4</sub>Ge<sub>1.6</sub>(PO<sub>4</sub>)<sub>3</sub> (LAGP) electrolyte and lithium are studied using in situ transmission electron microscopy and ex situ techniques. The reaction of lithium with LAGP causes amorphization and volume expansion, which induce mechanical stress and fracture of the SSE along with a massive increase in impedance. The evolved interphase has a nonuniform morphology at high currents, which causes accelerated chemo-mechanical failure. This work demonstrates that the



current-dependent nature of the reaction at the SSE/Li interface plays a crucial role in determining chemo-mechanical degradation mechanisms, with implications for understanding and controlling degradation in a wide variety of SSE materials with unstable interfaces.

he lithium metal anode has long been a target for implementation in secondary batteries, as it has a high theoretical specific capacity (3860 mAh g<sup>-1</sup>) and a low potential (-3.04 V vs SHE), making it a desirable material for batteries with higher energy density. However, attempts to use a lithium metal anode in liquid-based electrolytes have failed because of the dendritic electrodeposition of lithium, which can short circuit the cell and increase the risk of fires induced by thermal runaway. A potential alternative route to enabling lithium metal anodes is to use a solid-state electrolyte (SSE) that can impede dendrite growth while still facilitating rapid ion transport. Numerous Li<sup>+</sup>-ion conducting oxideand sulfide-based SSEs with ionic conductivity >0.1 mS cm<sup>-1</sup> have been discovered and investigated for lithium-ion battery applications.

Several issues have held back the development of solid-state batteries. Multiple research groups have reported short-circuiting of the garnet SSE Li<sub>7</sub>La<sub>3</sub>Zr<sub>2</sub>O<sub>12</sub> (LLZO) when cycled with current densities greater than a critical value due to

lithium growth through the material, even though LLZO has a shear modulus greater than 10 times that of lithium metal.  $^{11-15}$  This behavior has also been observed at relatively high current densities in other SSE materials, including glassy Li<sub>2</sub>S–P<sub>2</sub>S<sub>5</sub> and polycrystalline  $\beta$ -Li<sub>3</sub>PS<sub>4</sub>. Additionally, the vast majority of oxide- and sulfide-based SSE materials have been predicted to be thermodynamically unstable in contact with lithium metal, which likely results in the formation of a new phase or mixture of phases at the interface (an *interphase* layer) that exhibits different properties.  $^{17-22}$  Such interphases may have poor ionic conductivity, resulting in high interfacial impedance and cell degradation.

While understanding the formation of interphases is important for the reliable use of lithium metal in solid-state batteries, <sup>23</sup> only a few studies have directly investigated the

Received: January 13, 2019 Accepted: January 28, 2019



<sup>&</sup>lt;sup>†</sup>School of Materials Science and Engineering, Georgia Institute of Technology, 771 Ferst Drive, Atlanta, Georgia 30332, United States

<sup>&</sup>lt;sup>‡</sup>George W. Woodruff School of Mechanical Engineering, Georgia Institute of Technology, 801 Ferst Drive, Atlanta, Georgia 30332, United States

<sup>§</sup>Center for Nanophase Materials Sciences, Oak Ridge National Laboratory, One Bethel Valley Road, Oak Ridge, Tennessee 37831, United States

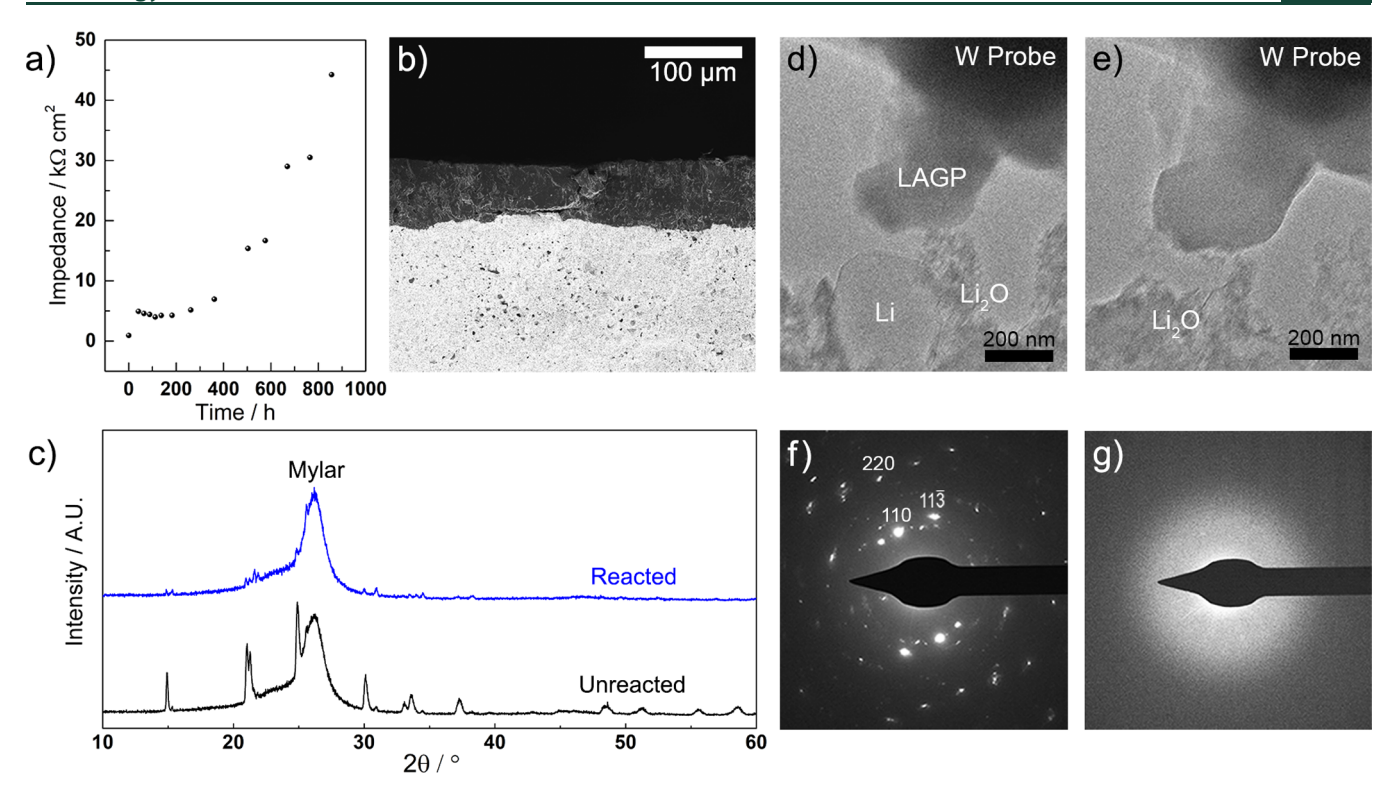


Figure 1. (a) Plot of impedance versus time for a Li/LAGP/Li symmetric cell held at open circuit. (b) Cross-sectional SEM image of the interphase formed by chemical reaction. (c) Ex situ glancing angle XRD pattern of unreacted LAGP and LAGP that was chemically reacted for  $\sim$ 170 h. The broad peak at  $\sim$ 26.5° is from the Mylar film covering the samples to prevent air exposure. (d-g) In situ TEM results of the reaction of an LAGP particle with lithium. (d) Image of an unreacted LAGP particle before contact with lithium. (e) Image of the same LAGP particle after being contacted and reacting with lithium. After lithiation, the particle expanded in volume and the lithium crystal disappeared. (f) SAED pattern of an unreacted LAGP particle. (g) SAED pattern of the same particle after lithiation.

phase(s) that form at SSE/Li interfaces.<sup>24-27</sup> Even more critically, we lack comprehensive understanding of how the formation of an interphase during electrochemical cycling impacts the chemo-mechanical stability of solid-state batteries. Chemo-mechanical degradation pathways could include material fracture due to lithium penetration<sup>16</sup> as well as impedance increases due to interphase growth. Elucidating these degradation pathways during cycling of unstable SSEs is a key step toward engineering interfaces to prevent degradation. Design of stable interfaces will enable a broader range of candidate electrolyte materials for solid-state lithium metal batteries beyond the handful that are thermodynamically stable in contact with Li. To achieve this goal, it is necessary to probe how Li/SSE interfaces evolve during electrochemical cycling and to understand how the formation of an interphase is related to cell degradation. As in the case of lithium penetration, establishing a relationship between current density and cell degradation is also needed to understand the performance capabilities of unstable SSEs.

NASICON-type SSEs are a promising class of materials with relatively high ionic conductivity (~0.1–1 mS cm<sup>-1</sup>)<sup>7,28</sup> that have been shown to be chemically unstable in contact with lithium. Despite their instability at low potentials, they have relatively high oxidation potentials that provide better stability against cathodes compared to many other SSEs. They are also stable in air, whereas garnet and sulfide SSEs degrade upon exposure to humid atmospheres. While other SSEs, such as some sulfides, have higher conductivity, the advantages that NASICON materials provide are attractive for the development of a variety of battery systems. A recent study

on the chemical reaction between  $\operatorname{Li}_{1+x}\operatorname{Al}_x\operatorname{Ge}_{2-x}(\operatorname{PO}_4)_3$  (LAGP) and lithium showed that LAGP readily reacts at room temperature, which can drive fracture of LAGP. Stabilizing the Li/LAGP interface to prevent this reaction is therefore necessary to make LAGP a practical candidate for Li metal batteries. However, mechanical degradation due to electrochemical processes has been studied only under potentiostatic conditions and has not been directly linked to morphological or volumetric changes at the interface. Understanding the underlying phenomena that govern the (electro)chemical growth of the interphase, how this process is related to degradation, and the effects of current density on interphase formation and degradation is crucial to tailor electrochemically stable Li/LAGP interfaces.

Here, the (electro)chemical reaction mechanism between lithium and LAGP is investigated with in situ transmission electron microscopy (TEM) and ex situ techniques, and we show that the morphological evolution of the interphase during electrochemical cycling in symmetric cells is highly dependent on current density and that the interphase morphology controls chemo-mechanical failure. The chemically reacted interphase is found to be amorphous, which deviates from prior simulation predictions. <sup>19–21</sup> The interfacial reaction involves lithium insertion and volume expansion that induces mechanical stress and drives fracture within the ceramic SSE. Ultimately, a massive increase in impedance due to crack proliferation causes cells to fail, which fundamentally differs from the failure mechanism reported for other ceramic SSEs, such as garnet LLZO. These findings elucidate key degradation and failure mechanisms in this important class of SSEs, with

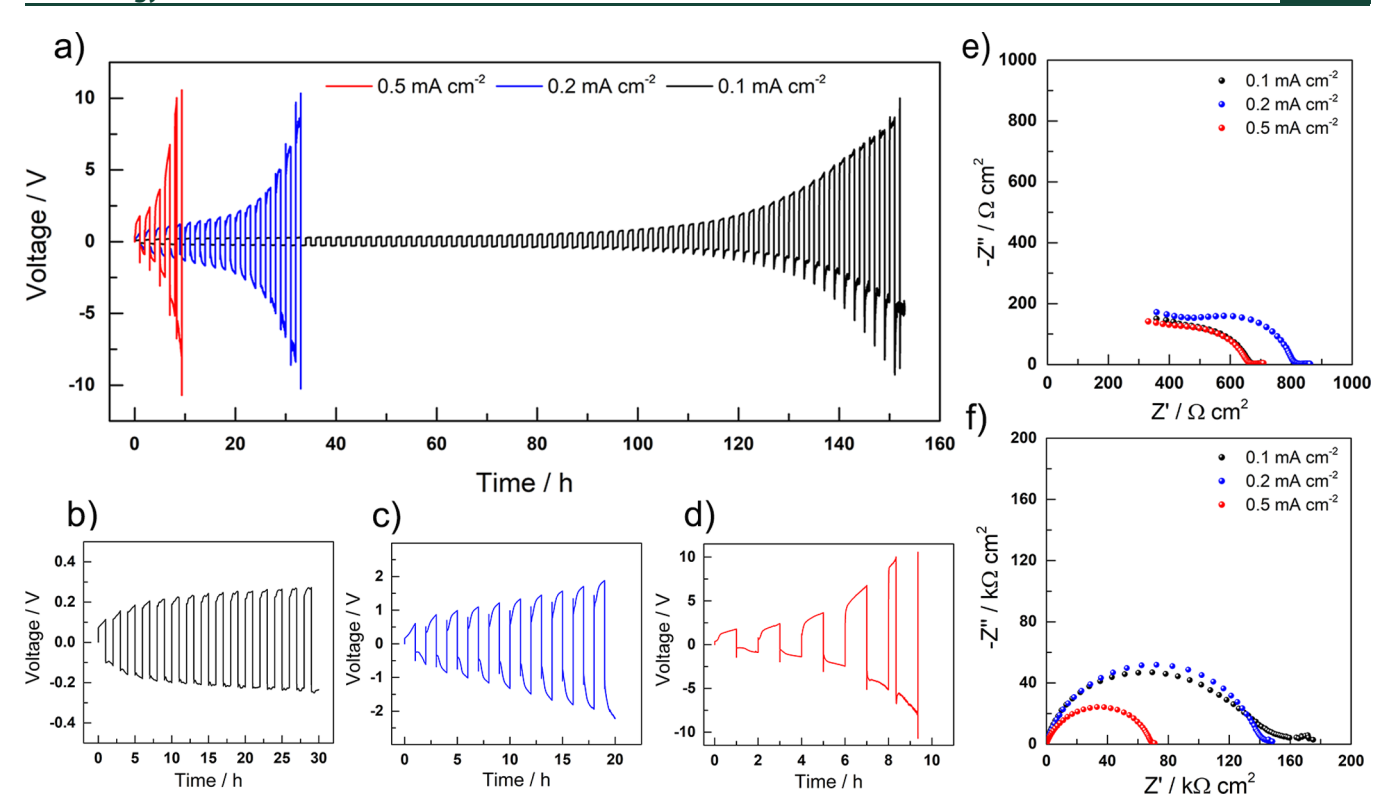


Figure 2. (a) Galvanostatic cycling of symmetric Li/LAGP/Li cells cycled to failure (defined to be  $\pm 10$  V) at 0.1 mA cm<sup>-2</sup> (black), 0.2 mA cm<sup>-2</sup> (blue), and 0.5 mA cm<sup>-2</sup> (red). (b-d) Magnified plots of the galvanostatic traces presented in panel a at early cycling times. (e) Impedance spectra of each cell in panel a prior to cycling. (f) Impedance spectra of each cell after galvanostatic cycling to failure.

implications for the many SSEs that form nonpassivating interphases in contact with lithium metal.

LAGP powder was prepared using a sol-gel procedure and uniaxially pressed and sintered to form pellets with the expected rhombohedral structure (space group  $R\overline{3}c$ ), as shown in Figure S1 in the Supporting Information.<sup>34</sup> The density of synthesized LAGP was measured to be ~88%, and the ionic conductivity was typically 0.1-0.3 mS cm<sup>-1</sup> based on electrochemical impedance spectroscopy (EIS) measurements of pellets with Au electrodes (Figure S2). Using this LAGP material, the chemical reaction between the SSE and lithium was investigated. Symmetric Li/LAGP/Li coin cells were fabricated and left to rest at open circuit. After 36 days, the impedance increased from 926  $\Omega$  cm<sup>2</sup> to 44 200  $\Omega$  cm<sup>2</sup> (Figures 1a and S3a). Upon opening the cell, we observed that the LAGP pellet had fractured into many pieces, as has been observed in previous work.<sup>33</sup> Scanning electron microscopy (SEM) images of the cross section and surface of LAGP that was reacted for ~300 h, shown in Figures 1b and S3b, revealed that a relatively uniform interphase with an average thickness of 61  $\pm$  8  $\mu$ m had formed on the surface of the LAGP. Energy-dispersive X-ray spectroscopy (EDS) mapping (Figure S4) confirmed that the reacted region contained Ge, Al, and P, indicating that it was not residual lithium metal.

The crystal structure of the reacted interphase was characterized using ex situ X-ray diffraction (XRD) and Raman spectroscopy. Figure 1c compares the XRD patterns of unreacted and reacted LAGP collected using a fixed X-ray incidence angle of 1° to minimize the signal from the unreacted LAGP beneath the interphase. While the pristine LAGP exhibits diffraction peaks characteristic of its rhombohe-

dral crystal structure, the XRD pattern after reaction does not show any additional peaks. Instead, the reacted material shows diminished peak intensities, suggesting that the interphase is amorphous. Ex situ Raman spectroscopy also showed that the reacted interphase did not exhibit Raman modes (Figure S3c), further supporting the conclusion that the phase is amorphous.

To investigate nanoscale reaction processes and morphological changes between lithium and LAGP, in situ TEM was employed using a specialized probing/electrical biasing holder. Related in situ TEM experiments have previously been used to study the electrochemical lithiation of battery electrode materials, 35-37 and these techniques have recently been applied to study other SSE materials. 24,25 Here, LAGP particles were brought into direct contact with pure lithium metal within the TEM while a bias was applied. During this process, the chemical reaction between the materials was observed in real time (see Experimental Section in the Supporting Information for details). A selected-area electron diffraction (SAED) pattern of a pristine LAGP particle (Figure S5) confirms that these particles are crystals with the expected rhombohedral structure. Figure 1d shows an LAGP particle before being contacted by lithium metal. Within tens of seconds after contact (Figure 1e), the imaged area of the LAGP particle expanded by ~38%, and the particle exhibited lighter contrast. Furthermore, the lithium particle clearly decreased in volume during the reaction, indicating that lithium diffused into LAGP. This observation provides direct evidence that the reaction of LAGP with lithium causes volume expansion, resulting in the rounded morphology of the reacted grains seen in Figure S3b. SAED was also performed before and after reaction of LAGP particles. Figure 1f shows an SAED pattern of a pristine LAGP particle prior to reaction; the SAED

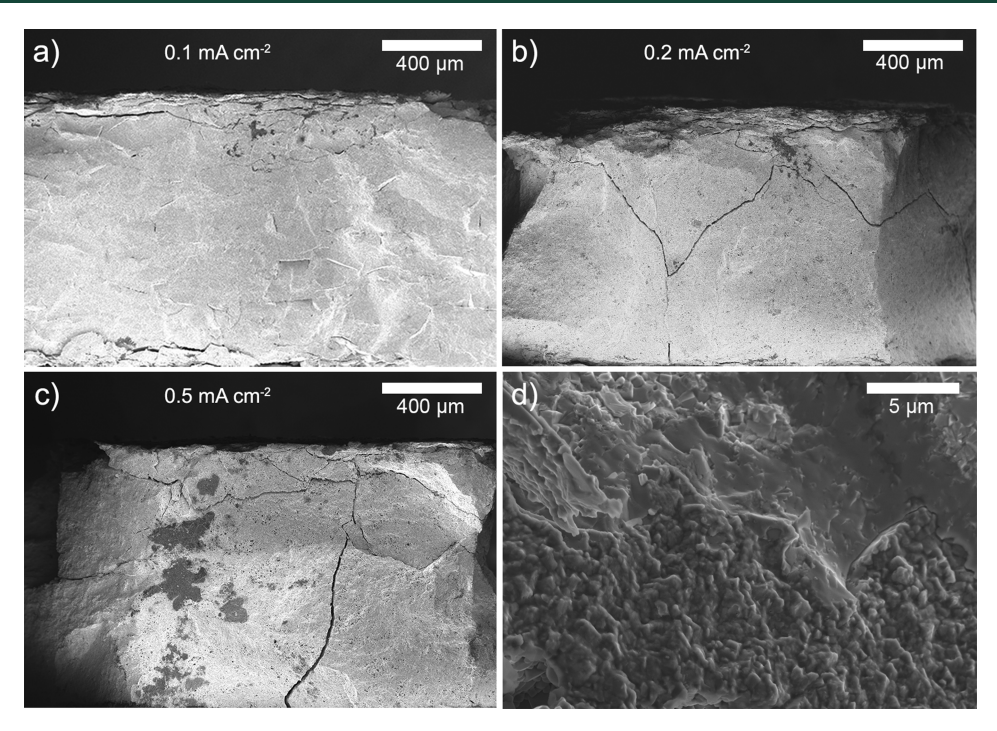


Figure 3. (a-c) Low-magnification cross-sectional SEM images of LAGP cycled until failure at (a) 0.1 mA cm<sup>-2</sup>, (b) 0.2 mA cm<sup>-2</sup>, and (c) 0.5 mA cm<sup>-2</sup>. The darker regions are the reacted interphase that has grown into the bulk of the LAGP. (d) Higher-magnification SEM image of the interphase grown deep within LAGP.

pattern in Figure 1g is from the same particle after reaction had occurred. The reacted pattern shows diffuse intensity but no diffraction spots, confirming that the reacted phase is amorphous. The possibility of the electron beam itself causing amorphization was ruled out by exposing pristine LAGP particles to the beam for similar amounts of time as in the lithiation experiments, which did not cause amorphization.

The combination of in situ TEM, ex situ XRD, and ex situ Raman spectroscopy confirms that the reaction at the LAGP/ Li interface results in the formation of an amorphous phase during lithiation and volume expansion. This finding is consistent with prior work in which XRD results suggested an amorphization process.<sup>33</sup> The formation of an amorphous phase rather than a crystalline phase is important because density functional theory studies have predicted the formation of crystalline products (Li<sub>9</sub>Al<sub>4</sub>, Li<sub>15</sub>Ge<sub>4</sub>, Li<sub>3</sub>P, and Li<sub>2</sub>O) as the thermodynamically stable phases at this interface. 19-21 This reaction has also been experimentally shown to involve the reduction of Ge<sup>4+</sup> to form metallic Ge.<sup>29</sup> Our results show that a metastable amorphous phase forms during the reduction of LAGP with lithium at room temperature. This amorphous phase likely exhibits different ionic and electronic transport characteristics compared to the predicted mixture of crystalline phases, which can result in differing growth behavior and stability of the interface. The amorphization process observed here likely occurs because of the complex dynamics required for the formation of multiple binary crystalline phases; instead, the formation of a single amorphous phase seems to be kinetically favored. Additionally, the amorphous phase may also be energetically preferred if the interfaces between the thermodynamically predicted phases exhibit high energy.

We next investigated the relationship between the interfacial reaction and chemo-mechanical failure mechanisms of symmetric Li/LAGP/Li cells during electrochemical cycling. Although other work has recently demonstrated the effective-

ness of protection layers in extending the lifetime of symmetric Li/LAGP/Li cells, <sup>38</sup> little is known about how NASICON-based cells electrochemically degrade and how this process is influenced by current density. Porz et al. found that the failure mechanism of garnet and sulfide SSEs at relatively high current densities is related to crack initiation and propagation caused by the growth of lithium filaments within the SSEs, indicating that this mechanism may be found in a variety of materials. <sup>16</sup> The persistent growth of these cracks allows for the filaments to penetrate through the SSE, eventually resulting in a short circuit. However, it is unknown whether symmetric Li/LAGP/Li cells undergo electrochemical degradation processes that are similar to these other SSEs.

The effect of applied current on chemo-mechanical degradation was studied by galvanostatically cycling Li/ LAGP/Li symmetric cells at different current densities (0.1, 0.2, and 0.5 mA cm<sup>-2</sup>) until failure occurred. Short circuiting was not observed for any cell tested at these current densities. Instead, failure involved a significant increase in overpotential for all three current densities (Figure 2a), with an overpotential of ±10 V being used as a failure criterion. However, the cell cycled at the lowest current density exhibited relatively stable cycling for ~100 h before a significant rise in overpotential, while the cell cycled at 0.5 mA cm<sup>-2</sup> rapidly deteriorated in less than 10 h (see magnified cycling data in Figure 2b-d). The absence of short circuits indicates that failure in LAGP symmetric cells at these current densities is not governed by the growth of lithium filaments through the SSE. A comparison of the initial and final EIS spectra in Figure 2e,f shows that the impedance increased dramatically for all three current densities. After cycling to failure, the cells were opened and the LAGP pellets were found to be fractured for all current densities tested. The chemical reaction (Figure 1) was also found to induce fracture, but electrochemical cycling significantly accelerated the rise in impedance compared to

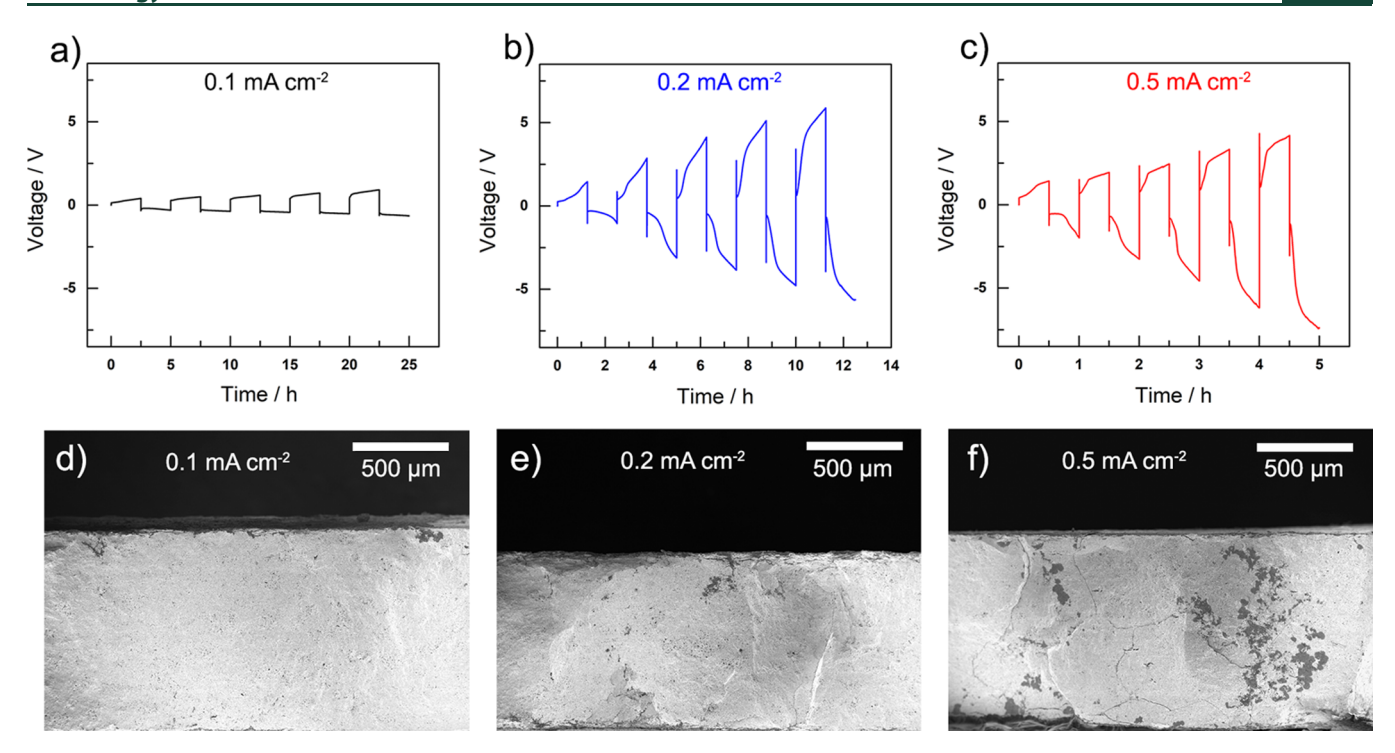


Figure 4. Galvanostatic cycling of symmetric Li/LAGP/Li cells cycled at (a)  $0.1 \text{ mA cm}^{-2}$ , (b)  $0.2 \text{ mA cm}^{-2}$ , and (c)  $0.5 \text{ mA cm}^{-2}$ . For all three current densities, the capacity per half-cycle was  $0.25 \text{ mAh cm}^{-2}$  and the total capacity was  $2.5 \text{ mAh cm}^{-2}$ . (d-f) Cross-sectional SEM images of LAGP after cycling with the same amount of Li<sup>+</sup> passed. The top surfaces of the pellets are visible in panels d and f because of sample orientation in the microscope.

the chemical reaction process. These results indicate that LAGP, and likely other SSE materials that readily react with lithium, can undergo different failure mechanisms than the short circuiting previously reported for LLZO.

Characterization of cycled LAGP was carried out to further understand failure mechanisms. Figure 3a-c shows crosssectional SEM images of LAGP cycled until failure at 0.1, 0.2, and 0.5 mA cm<sup>-2</sup>. Comparison of the low-magnification images at each current density shows that the morphology of the interphase became increasingly nonuniform at higher current densities. At 0.1 mA cm<sup>-2</sup>, the cross section exhibited a thin interphase at the interface with an approximate thickness of 15  $\mu$ m, along with horizontal cracks near the interface and some regions of nonuniform growth into the bulk (Figure 3a). A similar interphase was seen in the cross section of the pellet cycled at 0.2 mA cm<sup>-2</sup>, as shown in Figure 3b. However, in cells that were cycled to failure at 0.5 mA cm<sup>-2</sup>, the growth of the darker reacted phase was highly nonuniform and penetrated deep into the pellet (Figure 3c). The image in Figure 3d shows that the smooth morphology of this penetrating interphase resembled the previously discussed chemically reacted interphase (Figure 1b).

The significant increase in cell impedance during cycling, and thus cell failure, likely occurred because of the formation of cracks instead of being directly due to the impedance of the interphase. Cracks in the pellets prevent ion flow by isolating portions of the SSE, leading to increased impedance and overpotential. In contrast, the reacted interphase seemingly permits ion flow with only moderate impedance, because the cells can be stably cycled at low current densities. The mechanical stress necessary to drive crack formation and propagation is presumably caused by the volume expansion during reaction to form the interphase, as directly observed in

Figure 1. The reacted interphase expands under the constraint of the LAGP matrix and is thus under compression, while tensile stress is exerted on the unreacted LAGP. The magnitude of the expansion after ~300 h of chemical reaction is estimated to be ~130% based on SEM data of the height of the reacted region. With this in mind, the differences in the extent of reaction and the morphology of the reacted interphase at low and high current densities likely determine the time to chemo-mechanical failure (as shown in Figure 3). Higher currents cause more nonuniform interphase growth that penetrates deeper into the SSE, creating highly localized and nonuniform stress distributed throughout the pellet. This could result in stress concentrations that drive fracture more readily, thus explaining why fracture occurs more quickly at higher current densities.

From the data in Figures 2 and 3, it is unclear whether the differences in the time to failure and the extent of growth of the interphase were caused by different current densities or by the total amount of lithium transferred in each experiment. To decouple these two parameters, we cycled symmetric Li/ LAGP/Li cells using the same capacity per cycle and the same total capacity for all three current densities. In these experiments, the capacity per half-cycle was 0.25 mAh cm<sup>-2</sup> and the total capacity over the course of the experiment was 2.5 mAh cm<sup>-2</sup>. Figure 4a-c shows the galvanostatic traces for cells cycled at each current density (0.1, 0.2, and 0.5 mA cm<sup>-2</sup>), and Figure 4d-f shows SEM images detailing the extent of reaction throughout the cross section of each sample. The trace from the cell cycled at 0.1 mA cm<sup>-2</sup> (Figure 4a) shows that the overpotential grows to be higher than the previous data in Figure 3a,b because of the longer time per cycle, but the cell is still fairly stable. The SEM image from this cell (Figure 4d) shows that the interphase is primarily

maintained near the top surface, with some small regions of the reacted phase penetrating into the near-surface bulk region. In contrast, the cells cycled at currents of 0.2 and 0.5 mA cm<sup>-2</sup> rapidly reached high overpotentials and exhibited poor electrochemical stability. Despite the similar galvanostatic signatures (Figure 4b,c), the cell cycled at 0.5 mA cm<sup>-2</sup> exhibited substantially more growth of the reacted phase into the bulk of the LAGP pellet compared to the cell cycled at 0.2 mA cm<sup>-2</sup>. Having isolated the effects of current density from the total lithium transferred during cycling, these data clearly demonstrate that the spatial distribution of the reacted phase is highly dependent on the magnitude of the applied current density.

Although these results demonstrate that nonuniform interphase growth within LAGP causes mechanical degradation of symmetric Li/LAGP/Li cells, it is unclear from these data if this behavior would also occur in full cells. To explore interphase growth in a full lithium metal battery, we assembled cells with a lithium metal anode and a LiFePO4 (LFP) cathode. The cathode was fabricated by drop-casting a slurry containing LFP, poly(ethylene oxide) (PEO), LiTFSI salt, and Super P carbon onto the LAGP pellet and drying (the Supporting Information contains full details). Full cells were galvanostatically cycled at 60 °C between 2.5 and 4 V with a current density of 0.1 or 0.2 mA cm<sup>-2</sup>, as shown in Figure S6. The elevated cycling temperature was necessary because of the low ionic conductivity of the PEO in the cathode. SEM of the cross sections after cycling revealed that an interphase had formed at the Li/LAGP interface, but not at the LAGP/LFP interface (Figure S6). The higher temperature resulted in the accelerated growth of the interphase in these full cells as well as in symmetric cells cycled under the same temperature conditions. In both cases, the interphase that formed at a current density of 0.2 mA cm<sup>-2</sup> was largely uniform, but there were also regions that showed nonuniform growth (Figure S6). Currents higher than this unfortunately yielded very low specific capacity, making comparisons to higher current densities difficult. Although this higher temperature appears to alter the relationship between current density and interphase morphology, we believe that the similarities between the full cells and symmetric cells at 60 °C indicate that the degradation mechanisms we observed in roomtemperature symmetric cells are valid for full cells as well. Further comprehensive study is necessary to confirm this conclusion.

The transport properties of the interphase should play a key role in the interphase reaction process. If the interphase is electronically insulating but ionically conductive, then a selflimiting interphase layer is expected to form because of direct chemical reaction.<sup>20</sup> Instead, we observed continuous growth of the chemically formed interphase and nonuniform penetration during electrochemical cycling, which suggests that the interphase is a mixed ion and electron conductor. Previous XPS experiments on the chemical reaction between lithium and LAGP demonstrated that Ge4+ is reduced to Ge0 in the interphase, <sup>29</sup> which could give rise to increased electronic conductivity. However, the chemical nature of the electrochemically formed interphase has not been investigated. To compare the chemical nature of the chemical and electrochemical interphase, we conducted XPS experiments on (i) a chemically reacted sample that was contacted with lithium foil for ~25 h and (ii) an electrochemically reacted sample cycled at  $0.2 \text{ mA cm}^{-2}$  for  $\sim 25 \text{ h}$  in a symmetric cell. Ar

sputtering was used for depth profiling. Figure S7 shows the Ge 3d spectra at the surface and deeper within the interphase for the two different interphases. In both cases, the Ge in the interphase was reduced compared to the Ge<sup>4+</sup> in pristine LAGP. However, these data also show that the distribution of oxidation states in the two different interphases was different, with an increased fraction of species reduced beyond Ge<sup>2+</sup> in the electrochemical interphase. This difference could be explained by the fact that the electrochemical interphase is formed both by chemical diffusion (as in the chemical interphase) as well as additional reactions due electrochemical reduction. In both cases, however, mixed-conduction behavior was observed.

The ability to conduct both ions and electrons through the interphase would enable two electrochemical reduction pathways during cycling, as schematically shown in Figure 5.

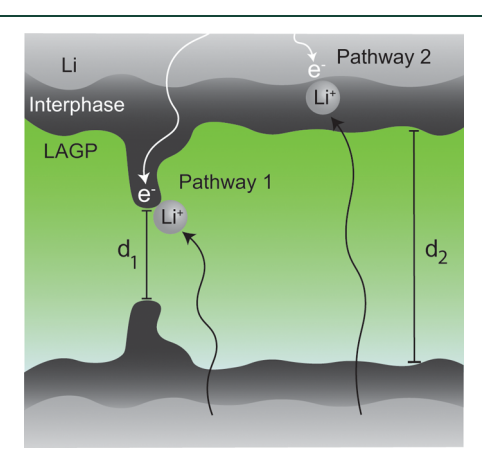


Figure 5. Schematic showing nonuniform interphase growth and possible reduction pathways in relation to the growth of the mixed-conducting interphase. Pathway 1 is the reduction of LAGP at the LAGP/interphase boundary via the transport of electrons through the mixed-conducting interphase. This pathway plays an important role in nonuniform growth of the interphase. Pathway 2 is the plating of lithium at the interphase/Li interface, which should not cause electrochemical growth of the interphase. Nonuniform growth is promoted via pathway 1 because nonuniform growth decreases the distance required for Li<sup>+</sup> transport (e.g.,  $d_1$  compared to  $d_2$ ), thereby locally lowering the resistance to ion conduction.

LAGP could be electrochemically reduced at the LAGP/ interphase boundary (reaction pathway 1 in Figure 5) by combining incoming Li<sup>+</sup> ions with electrons that have traversed the interphase. This reaction may occur via the direct electrochemical reduction of LAGP, or it could be a multistep process involving electrochemical reduction of ions to form lithium metal followed by chemical reaction with LAGP. Lithium plating at the LAGP/Li interface could also occur (reaction pathway 2 in Figure 5). The occurrence of this reaction pathway was confirmed in independent experiments in which custom cells with only a thin Au top contact were galvanostatically tested (Figure S8), revealing the growth of lithium metal at the Au contact. These two distinct reduction pathways are in competition with each other in this system, and it is likely that both processes occur simultaneously (depending on current density).

We hypothesize that the shift from uniform interphase growth seen in the chemical reaction to nonuniform growth observed after electrochemical cycling at higher currents is a

consequence of the mixed-conducting properties of the interphase that activate reaction pathway 1. In general, the resistance to ion transport across the SSE (and thus the portion of the overpotential due to ion transport) is lower when the ion transport length is shorter. The nonuniform growth of the interphase at higher currents likely arises because of the system acting to minimize the transport distance and the required overpotential for the electrochemical process. The reduction of LAGP at interphase protrusions (pathway 1 in Figure 5) allows for the continuous decrease of ion transport length. This promotion of shorter ion transport pathways is expected to be amplified at higher current densities because the overall overpotential is higher, leading to the significant nonuniformities observed in Figures 3c and 4f. In addition to this effect, reaction pathway 1 would also be promoted if the interphase electronic conductivity was higher than the interphase ionic conductivity; this phenomenon (which would also be exacerbated at higher currents) could also be playing a role.

LAGP is chemically and electrochemically reactive toward lithium, in contrast to SSEs that are more stable against lithium (such as LLZO) or SSEs that form a passivating interphase.<sup>39</sup> Lithium deposited at the SSE/Li interface in these cases is not consumed by chemical reaction, and the lithium can grow to mechanically penetrate the SSE. It is therefore apparent that the nature of the interphase reaction mechanism of an SSE with lithium impacts the growth of filaments through the material. Our results demonstrate that the current density, along with the properties of the interphase, are critical parameters in determining the electrochemical degradation mechanism of SSEs. At the current densities tested in this work, the growth of lithium filaments was not observed. This current density regime is comparable to the reported critical current densities for short circuits to form in LLZO-based symmetric cells (between 0.05 and 1 mA cm<sup>-2</sup>). 11,40-44 Despite comparable rates, the failure mechanism of LAGP deviates from garnet SSEs because of the continuous reactivity of the LAGP/Li interface. However, Porz et al. demonstrated that filaments can be formed in glassy Li<sub>2</sub>S-P<sub>2</sub>S<sub>5</sub>, which exhibits less stability against Li than garnets, when a very large current density (~10 mA cm<sup>-2</sup>) is applied. 16 It is reasonable then to expect that short-circuiting is possible in continuously reacting SSEs such as LAGP. However, the formation of lithium filaments in these materials may require such high current densities that overpotentials become unreasonably large for electrochemical cycling. Finally, despite the mechanistic differences between the growth of lithium filaments and the formation of nonuniform interphase regions, these mechanisms are related in the context of chemomechanical degradation because mechanical failure (fracture) occurs in both cases, and fracture depends on the mechanical properties of the SSE and the growing phase (either the reacted interphase or lithium metal).

As previously mentioned, the transport properties of the interphase strongly influence interphase growth behavior and degradation mechanisms in SSEs. Discovering or creating interphases on various SSEs with appropriate ionic and electronic conductivities to prevent the reduction of the SSE by lithium is critical for designing solid-state cells that can be reliably cycled over long periods of time. For example, engineering the surface of LAGP to create artificial interphases that are stable over time could prevent the buildup of stresses that lead to mechanical failure. This strategy has recently been

pursued with the primary goal of reducing interface resistance at LLZO/Li interfaces, 45-48 but going further to engineer interfaces in inherently unstable SSE materials is a promising route to increasing the number of electrolytes available for solid-state battery development. Furthermore, preventing the continuous formation of the interphase will also require consideration of the direct diffusion of Li species from lithium metal to react with the SSE, as occurs during the chemical reaction reported here. This pathway is often overlooked in the context of mixed-conducting interphase formation, but it also must be controlled for long-term stability.

This study has revealed reaction mechanisms at the LAGP/ Li interface and has linked current-dependent reaction processes to chemo-mechanical failure of solid-state cells. The chemical and electrochemical reactions at the LAGP/Li interface were investigated using in situ TEM and other ex situ techniques. The reaction of LAGP with lithium involves (electro)chemical reduction of the SSE to form an amorphous interphase. During this process, LAGP undergoes volume expansion due to the incorporation of lithium that causes the evolution of mechanical stress within bulk LAGP pellets and eventually induces fracture. Electrochemical cycling of symmetric Li/LAGP/Li cells showed that the impedance and overpotential increased with time until fracture-induced failure. Nonuniform growth of the reacted interphase occurred within the bulk of the SSE at higher currents, which can cause localized stress concentrations and accelerate mechanical failure of the LAGP. This work demonstrates that the continuous reaction of the LAGP/Li interface is the root cause of the chemo-mechanical degradation of this material during cycling, and the improved understanding of these chemical and electrochemical interfacial reactions will hopefully spur development of strategies to combat degradation processes in a variety of SSE materials.

### ASSOCIATED CONTENT

# S Supporting Information

The Supporting Information is available free of charge on the ACS Publications website at DOI: 10.1021/acsenergy-lett.9b00093.

Full experimental details and additional data (PDF)

## AUTHOR INFORMATION

# **Corresponding Author**

\*E-mail: mattmcdowell@gatech.edu.

ORCID

Miaofang Chi: 0000-0003-0764-1567

Matthew T. McDowell: 0000-0001-5552-3456

Notes

The authors declare no competing financial interest.

# ■ ACKNOWLEDGMENTS

This material is based upon work supported by the National Science Foundation under Award No. DMR-1652471. A portion of this research was conducted at the Center for Nanophase Materials Sciences, which is a DOE Office of Science User Facility. This work was performed in part at the Georgia Tech Institute for Electronics and Nanotechnology, a member of the National Nanotechnology Coordinated Infrastructure, which is supported by the National Science Foundation (Grant ECCS-1542174).

### REFERENCES

(1) Lin, D.; Liu, Y.; Cui, Y. Reviving the Lithium Metal Anode for High-Energy Batteries. *Nat. Nanotechnol.* **2017**, *12*, 194–206.

- (2) Xu, W.; Wang, J.; Ding, F.; Chen, X.; Nasybulin, E.; Zhang, Y.; Zhang, J. G. Lithium Metal Anodes for Rechargeable Batteries. *Energy Environ. Sci.* **2014**, *7*, 513–537.
- (3) Aurbach, D.; Zinigrad, E.; Cohen, Y.; Teller, H. A Short Review of Failure Mechanisms of Lithium Metal and Lithiated Graphite Anodes in Liquid Electrolyte Solutions. *Solid State Ionics* **2002**, *148*, 405–416
- (4) Zhang, Z.; Shao, Y.; Lotsch, B. V.; Hu, Y.-S.; Li, H.; Janek, J.; Nazar, L. F.; Nan, C.-W.; Maier, J.; Armand, M.; et al. New Horizons for Inorganic Solid State Ion Conductors. *Energy Environ. Sci.* **2018**, *11*, 1945–1976.
- (5) Kerman, K.; Luntz, A.; Viswanathan, V.; Chiang, Y.-M.; Chen, Z. Review—Practical Challenges Hindering the Development of Solid State Li Ion Batteries. *J. Electrochem. Soc.* **2017**, *164*, A1731—A1744.
- (6) Kamaya, N.; Homma, K.; Yamakawa, Y.; Hirayama, M.; Kanno, R.; Yonemura, M.; Kamiyama, T.; Kato, Y.; Hama, S.; Kawamoto, K.; et al. A Lithium Superionic Conductor. *Nat. Mater.* **2011**, *10*, 682–686
- (7) Thokchom, J. S.; Kumar, B. Composite Effect in Superionically Conducting Lithium Aluminium Germanium Phosphate Based Glass-Ceramic. *J. Power Sources* **2008**, *185*, 480–485.
- (8) Murugan, R.; Thangadurai, V.; Weppner, W. Fast Lithium Ion Conduction in Garnet-Type Li<sub>7</sub>La<sub>3</sub>Zr<sub>2</sub>O<sub>12</sub>. *Angew. Chem., Int. Ed.* **2007**, *46*, 7778–7781.
- (9) Seino, Y.; Ota, T.; Takada, K.; Hayashi, A.; Tatsumisago, M. A Sulphide Lithium Super Ion Conductor Is Superior to Liquid Ion Conductors for Use in Rechargeable Batteries. *Energy Environ. Sci.* **2014**, *7*, 627–631.
- (10) Meesala, Y.; Jena, A.; Chang, H.; Liu, R. S. Recent Advancements in Li-Ion Conductors for All-Solid-State Li-Ion Batteries. ACS Energy Lett. 2017, 2, 2734–2751.
- (11) Sharafi, A.; Meyer, H. M.; Nanda, J.; Wolfenstine, J.; Sakamoto, J. Characterizing the Li- Li<sub>7</sub>La<sub>3</sub>Zr<sub>2</sub>O<sub>12</sub> Interface Stability and Kinetics as a Function of Temperature and Current Density. *J. Power Sources* **2016**, 302, 135–139.
- (12) Ren, Y.; Shen, Y.; Lin, Y.; Nan, C. W. Direct Observation of Lithium Dendrites Inside Garnet-Type Lithium-Ion Solid Electrolyte. *Electrochem. Commun.* **2015**, *57*, 27–30.
- (13) Aguesse, F.; Manalastas, W.; Buannic, L.; Del Amo, J. M. L.; Singh, G.; Llordés, A.; Kilner, J. Investigating the Dendritic Growth During Full Cell Cycling of Garnet Electrolyte in Direct Contact with Li Metal. ACS Appl. Mater. Interfaces 2017, 9, 3808–3816.
- (14) Cheng, E. J.; Sharafi, A.; Sakamoto, J. Intergranular Li Metal Propagation through Polycrystalline Li<sub>6.25</sub>Al<sub>0.25</sub>La<sub>3</sub>Zr<sub>2</sub>O<sub>12</sub> Ceramic Electrolyte. *Electrochim. Acta* **2017**, 223, 85–91.
- (15) Shen, F.; Dixit, M. B.; Xiao, X.; Hatzell, K. B. Effect of Pore Connectivity on Li Dendrite Propagation within LLZO Electrolytes Observed with Synchrotron X-Ray Tomography. *ACS Energy Lett.* **2018**, *3*, 1056–1061.
- (16) Porz, L.; Swamy, T.; Sheldon, B. W.; Rettenwander, D.; Frömling, T.; Thaman, H. L.; Berendts, S.; Uecker, R.; Carter, W. C.; Chiang, Y. M. Mechanism of Lithium Metal Penetration through Inorganic Solid Electrolytes. *Adv. Energy Mater.* **2017**, *7*, 1701003.
- (17) Xin, S.; You, Y.; Wang, S.; Gao, H. C.; Yin, Y. X.; Guo, Y. G. Solid-State Lithium Metal Batteries Promoted by Nanotechnology: Progress and Prospects. ACS Energy Lett. 2017, 2, 1385–1394.
- (18) Shen, Y.; Zhang, Y.; Han, S.; Wang, J.; Peng, Z.; Chen, L. Unlocking the Energy Capabilities of Lithium Metal Electrode with Solid-State Electrolytes. *Joule* **2018**, *2*, 1674–1689.
- (19) Zhu, Y.; He, X.; Mo, Y. First Principles Study on Electrochemical and Chemical Stability of Solid Electrolyte-Electrode Interfaces in All-Solid-State Li-Ion Batteries. *J. Mater. Chem. A* **2016**, 4, 3253–3266.
- (20) Zhu, Y.; He, X.; Mo, Y. Origin of Outstanding Stability in the Lithium Solid Electrolyte Materials: Insights from Thermodynamic

Analyses Based on First-Principles Calculations. ACS Appl. Mater. Interfaces 2015, 7, 23685–23693.

- (21) Richards, W. D.; Miara, L. J.; Wang, Y.; Kim, J. C.; Ceder, G. Interface Stability in Solid-State Batteries. *Chem. Mater.* **2016**, 28, 266–273.
- (22) Wu, E. A.; Kompella, C. S.; Zhu, Z.; Lee, J. Z.; Lee, S. C.; Chu, I. H.; Nguyen, H.; Ong, S. P.; Banerjee, A.; Meng, Y. S. New Insights into the Interphase Between the Na Metal Anode and Sulfide Solid-State Electrolytes: A Joint Experimental and Computational Study. *ACS Appl. Mater. Interfaces* **2018**, *10*, 10076–10086.
- (23) Augustyn, V.; McDowell, M. T.; Vojvodic, A. Towards an Atomistic Understanding of Solid-State Electrochemical Interfaces for Energy Storage. *Joule* **2018**, *2*, 2189–2193.
- (24) Ma, C.; Cheng, Y.; Yin, K.; Luo, J.; Sharafi, A.; Sakamoto, J.; Li, J.; More, K. L.; Dudney, N. J.; Chi, M. Interfacial Stability of Li Metal-Solid Electrolyte Elucidated via in Situ Electron Microscopy. *Nano Lett.* **2016**, *16*, 7030–7036.
- (25) Wang, Z.; Santhanagopalan, D.; Zhang, W.; Wang, F.; Xin, H. L.; He, K.; Li, J.; Dudney, N.; Meng, Y. S. In Situ STEM-EELS Observation of Nanoscale Interfacial Phenomena in All-Solid-State Batteries. *Nano Lett.* **2016**, *16*, 3760–3767.
- (26) Wenzel, S.; Randau, S.; Leichtweiß, T.; Weber, D. A.; Sann, J.; Zeier, W. G.; Janek, J. Direct Observation of the Interfacial Instability of the Fast Ionic Conductor  $\text{Li}_{10}\text{GeP}_2\text{S}_{12}$  at the Lithium Metal Anode. *Chem. Mater.* **2016**, *28*, 2400–2407.
- (27) Wenzel, S.; Weber, D. A.; Leichtweiss, T.; Busche, M. R.; Sann, J.; Janek, J. Interphase Formation and Degradation of Charge Transfer Kinetics between a Lithium Metal Anode and Highly Crystalline Li<sub>2</sub>P<sub>3</sub>S<sub>11</sub> Solid Electrolyte. *Solid State Ionics* **2016**, 286, 24–33.
- (28) Zhang, M.; Takahashi, K.; Imanishi, N.; Takeda, Y.; Yamamoto, O.; Chi, B.; Pu, J.; Li, J. Preparation and Electrochemical Properties of Li<sub>1+x</sub>Al<sub>x</sub>Ge<sub>2-x</sub>(PO<sub>4</sub>)<sub>3</sub> Synthesized by a Sol-Gel Method. *J. Electrochem. Soc.* **2012**, *159*, A1114–A1119.
- (29) Hartmann, P.; Leichtweiss, T.; Busche, M. R.; Schneider, M.; Reich, M.; Sann, J.; Adelhelm, P.; Janek, J. Degradation of NASICON-Type Materials in Contact with Lithium Metal: Formation of Mixed Conducting Interphases (MCI) on Solid Electrolytes. *J. Phys. Chem. C* 2013, 117, 21064–21074.
- (30) Wu, B.; Wang, S.; Lochala, J.; Desrochers, D.; Liu, B.; Zhang, W.; Yang, J.; Xiao, J. The Role of Solid Electrolyte Interphase Layer in Preventing Li Dendrite Growth in Solid-State Batteries. *Energy Environ. Sci.* **2018**, *11*, 1803–1810.
- (31) Sharafi, A.; Kazyak, E.; Davis, A. L.; Yu, S.; Thompson, T.; Siegel, D. J.; Dasgupta, N. P.; Sakamoto, J. Surface Chemistry Mechanism of Ultra-Low Interfacial Resistance in the Solid-State Electrolyte Li<sub>7</sub>La<sub>3</sub>Zr<sub>2</sub>O<sub>12</sub>. *Chem. Mater.* **2017**, *29*, 7961–7968.
- (32) Manthiram, A.; Yu, X.; Wang, S. Lithium Battery Chemistries Enabled by Solid-State Electrolytes. *Nat. Rev. Mater.* **2017**, *2*, 16103.
- (33) Chung, H.; Kang, B. Mechanical and Thermal Failure Induced by Contact Between a Li<sub>1.5</sub>Al<sub>0.5</sub>Ge<sub>1.5</sub>(PO<sub>4</sub>)<sub>3</sub> Solid Electrolyte and Li Metal in an All Solid-State Li Cell. *Chem. Mater.* **2017**, *29*, 8611–8619.
- (34) Alami, M.; Brochu, R.; Soubeyroux, J. L.; Gravereau, P.; Le Flem, G.; Hagenmuller, P. Structure and Thermal Expansion of LiGe<sub>2</sub>(PO<sub>4</sub>)<sub>3</sub>. *J. Solid State Chem.* **1991**, *90*, 185–193.
- (35) Yuan, Y.; Amine, K.; Lu, J.; Shahbazian-Yassar, R. Understanding Materials Challenges for Rechargeable Ion Batteries with in Situ Transmission Electron Microscopy. *Nat. Commun.* **2017**, *8*, 15806
- (36) Boebinger, M. G.; Yeh, D.; Xu, M.; Miles, B. C.; Wang, B.; Papakyriakou, M.; Lewis, J. A.; Kondekar, N. P.; Cortes, F. J. Q.; Hwang, S.; et al. Avoiding Fracture in a Conversion Battery Material through Reaction with Larger Ions. *Joule* **2018**, *2*, 1783–1799.
- (37) Boebinger, M. G.; Xu, M.; Ma, X.; Chen, H.; Unocic, R. R.; McDowell, M. T. Distinct Nanoscale Reaction Pathways in a Sulfide Material for Sodium and Lithium Batteries. *J. Mater. Chem. A* **2017**, *5*, 11701–11709.
- (38) Liu, Y.; Li, C.; Li, B.; Song, H.; Cheng, Z.; Chen, M.; He, P.; Zhou, H. Germanium Thin Film Protected Lithium Aluminum

Germanium Phosphate for Solid-State Li Batteries. *Adv. Energy Mater.* **2018**, *8*, 1702374.

- (39) Schwöbel, A.; Hausbrand, R.; Jaegermann, W. Interface Reactions between LiPON and Lithium Studied by In-Situ X-Ray Photoemission. *Solid State Ionics* **2015**, *273*, 51–54.
- (40) Basappa, R. H.; Ito, T.; Yamada, H. Contact between Garnet-Type Solid Electrolyte and Lithium Metal Anode: Influence on Charge Transfer Resistance and Short Circuit Prevention. *J. Electrochem. Soc.* **2017**, *164*, A666–A671.
- (41) Hongahally Basappa, R.; Ito, T.; Morimura, T.; Bekarevich, R.; Mitsuishi, K.; Yamada, H. Grain Boundary Modification to Suppress Lithium Penetration through Garnet-Type Solid Electrolyte. *J. Power Sources* **2017**, *363*, 145–152.
- (42) Cheng, L.; Chen, W.; Kunz, M.; Persson, K.; Tamura, N.; Chen, G.; Doeff, M. Effect of Surface Microstructure on Electrochemical Performance of Garnet Solid Electrolytes. *ACS Appl. Mater. Interfaces* **2015**, *7*, 2073–2081.
- (43) Sharafi, A.; Haslam, C. G.; Kerns, R. D.; Wolfenstine, J.; Sakamoto, J. Controlling and Correlating the Effect of Grain Size with the Mechanical and Electrochemical Properties of Li<sub>7</sub>La<sub>3</sub>Zr<sub>2</sub>O<sub>12</sub> Solid-State Electrolyte. *J. Mater. Chem. A* **2017**, *5*, 21491–21504.
- (44) Taylor, N. J.; Stangeland-Molo, S.; Haslam, C. G.; Sharafi, A.; Thompson, T.; Wang, M.; Garcia-Mendez, R.; Sakamoto, J. Demonstration of High Current Densities and Extended Cycling in the Garnet Li<sub>7</sub>La<sub>3</sub>Zr<sub>2</sub>O<sub>12</sub> Solid Electrolyte. *J. Power Sources* **2018**, 396, 314–318.
- (45) Han, X.; Gong, Y.; Fu, K.; He, X.; Hitz, G. T.; Dai, J.; Pearse, A.; Liu, B.; Wang, H.; Rubloff, G.; et al. Negating Interfacial Impedance in Garnet-Based Solid-State Li Metal Batteries. *Nat. Mater.* **2016**, *16*, 572–579.
- (46) Luo, W.; Gong, Y.; Zhu, Y.; Fu, K. K.; Dai, J.; Lacey, S. D.; Wang, C.; Liu, B.; Han, X.; Mo, Y.; et al. Transition from Superlithiophobicity to Superlithiophilicity of Garnet Solid-State Electrolyte. *J. Am. Chem. Soc.* **2016**, *138*, 12258–12262.
- (47) Luo, W.; Gong, Y.; Zhu, Y.; Li, Y.; Yao, Y.; Zhang, Y.; Fu, K. K.; Pastel, G.; Lin, C. F.; Mo, Y.; et al. Reducing Interfacial Resistance between Garnet-Structured Solid-State Electrolyte and Li-Metal Anode by a Germanium Layer. *Adv. Mater.* **2017**, *29*, 1606042.
- (48) Shao, Y.; Wang, H.; Gong, Z.; Wang, D.; Zheng, B.; Zhu, J.; Lu, Y.; Hu, Y. S.; Guo, X.; Li, H.; et al. Drawing a Soft Interface: An Effective Interfacial Modification Strategy for Garnet-Type Solid-State Li Batteries. ACS Energy Lett. 2018, 3, 1212–1218.